COMMUNICATIONS PHYSICS

ARTICLE

https://doi.org/10.1038/s42005-020-00455-6 OPEN

Bi-reflection of spin waves

Tomosato Hioki [1✉], Yusuke Hashimoto[2] & Eiji Saitoh[2,3]

When a light wave is refracted at a boundary between two different media, it may split into two rays due to optical anisotropy, a phenomenon called birefringence. On the other hand, for a reflected light wave in an ordinary medium, the angle of reflection is always the same as the incident angle as expected from the law of reflection. Here, we report the observation of a split of reflected spin-waves, or bi-reflection of spin-waves, where a spin-wave refers to a wavy motion of electron spins in a magnetic material. We measured the spin-wave propagation in a magnetic garnet $Lu_2Bi_1Fe_{3.4}Ga_{1.6}O_{12}$ by using time-resolved magneto-optical microscopy and found that the spin-wave splits in two as a result of reflection at the sample edge of an out-of-plane magnetized film. Systematic measurements combined with calculations unveiled that the bi-reflection is due to the hybridization with elastic waves.

[1] Institute for Materials Research, Tohoku University, Sendai 980-8577, Japan. [2] Advanced Institute for Materials Research, Tohoku University, Sendai 980-8577, Japan. [3] Department of Applied Physics, Faculty of Engineering, The University of Tokyo, Tokyo 113-8656, Japan. ✉email: tomosato.hioki.d7@tohoku.ac.jp

In an optically anisotropic medium, the velocity of a wave of light depends on its polarization direction[1]. Owing to the difference in the velocity, there are two independent propagation modes of a light wave in the medium: ordinary and extraordinary rays. When an unpolarized light wave enters into such an anisotropic medium from an isotropic one, a refracted light wave splits into two rays depending on the polarization (Fig. 1a). In the case of reflection, the reflected light wave does not split into two, unless the boundary normal and an optical axis in the anisotropic medium satisfy a particular condition imposed by symmetry consideration (Fig. 1b)[2,3].

In a magnetic material, a collective motion of electron spins forms a wave: a spin wave, which can carry information as a form of spin angular momentum[4–7]. Just like a light wave, a spin wave refracts and reflects in a magnetic material[8–10]. Although a pure spin wave does not carry a polarization degree of freedom, it can hybridize with an elastic wave via the magneto-elastic coupling, and inherit a mode degree of freedom from an elastic wave, that is, longitudinal and transverse modes, when the frequency and wavelength of spin waves are matched with that of elastic waves[11–18]. For the hybridized waves, the two propagation modes can convert to each other when translational symmetry is broken down, because the two modes are no longer eigenstates[19,20]. The conversion may occur at any types of boundaries in isotropic materials, including, but not limited to, a sample edge. Contrary to the light-wave split, the materials can be either isotropic or anisotropic to observe the conversion. As a result of the conversion, when a single-mode hybridized spin wave meets a sample edge, a reflected wave can split into two different modes: bi-reflection of spin waves.

Here we report the observation of bi-reflection of spin waves as a result of hybridization with elastic waves (Fig. 1c). By using time-resolved magneto-optical (TRMO) microscopy, we demonstrated that the magneto-elastic coupling induces a split of a reflected spin wave. The TRMO microscopy visualizes the spin orientation at different positions on a sample with high spatial resolution and picosecond time resolution (Fig. 2a)[21,22]. In the TRMO microscopy, two beams from a pulse laser source are used to excite and observe spin dynamics, which are called pump and probe beams, respectively. By the incidence of the pump beam, spin waves are excited through the photo-induced demagnetization and/or expansion[23–25]. By sweeping time delay between the pump and probe beams, one can obtain images of spin distribution at different times (see "Methods"). In the present study, the TRMO microscopy measures magneto-optical Faraday rotation, and thus it is sensitive to the out-of-plane component of magnetization[21]. We measured spin-wave propagation dynamics in a ferrimagnetic garnet ($Lu_2Bi_1Fe_{3.4}Ga_{1.6}O_{12}$) film. This material is suitable for TRMO microscopy because it has a larger magneto-optical effect

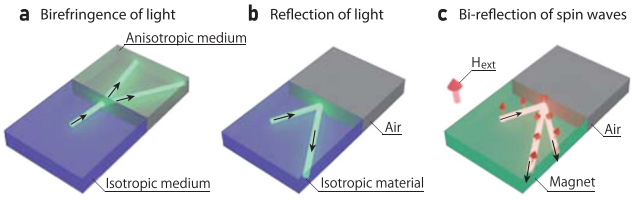

Fig. 1 Concept of bi-reflection. a A schematic of birefringence of a light. The transmitted light splits into two depending on the light polarization. **b** A schematic of reflection of a light. The light is totally reflected back at a boundary between materials. When boundary normal and an optical axis satisfies particular relation, reflected light wave may split into two. **c** A schematic of bi-reflection of spin waves. Spin waves, a collective wavy motion of electron spins in a magnetic material, reflect and split into two rays at the edge of out-of-plane magnetized film.

than yittrium iron garnet, one of the traditional materials for investigating spin-wave dynamics (see "Methods")[26,27]. To observe reflection of spin waves, the propagation direction of a spin wave is determined by shaping the focus of the pump beam into an ellipse[28,29]. During the measurement, an external magnetic field is applied along the z-direction to control the magnetization orientation between the out-of-plane and in-plane orientation. All the measurements were performed at room temperature.

Results

Magneto-optical imaging of bi-reflection of spin waves. Figure 2b–d shows the TRMO images obtained from an out-of-plane magnetized sample under the field $H = 1.35$ kOe at different values of time delay after the laser excitation. In these images, we clearly see propagation of a plane spin wave excited by the pulse laser. Importantly, we found that the reflected wave splits into two waves, showing bi-reflection of spin waves. The wavevectors of the split waves are referred as $\mathbf{k}_1$ and $\mathbf{k}_2$, respectively, in Figs. 2b–d. While $\mathbf{k}_1$ mode has the reflection angle same as the incident angle, $\mathbf{k}_2$ mode has much less reflection angle. $\mathbf{k}_2$ mode also has a shorter wavelength compared with the incident wave and $\mathbf{k}_1$ mode, meaning that $\mathbf{k}_2$ mode is owing to extraordinary reflection of spin waves.

The observed split of spin waves is consistent with the expected property for the bi-reflection. Due to the continuity of spin-wave phase at a boundary, the wavevector component along the sample edge should be kept the same during the reflection. The wavevector of reflected spin waves is analyzed by using the spin wave tomography (SWaT)[21], which gives spin-wave amplitude in the wavevector-frequency space based on the Fourier analysis at an arbitrary time range[21,24] (see "Methods"). Fig. 3a shows a cross-sectional view of the SWaT spectra on the isofrequency plane of $f = 1.53$ GHz obtained from an out-of-plane magnetized film. Before the spin wave meets the boundary, we see a single spectral peak corresponding to the incident wave (Fig. 3a). On the other hand, two distinctive spectral peaks appear after the incidence, corresponding to the $\mathbf{k}_1$ and $\mathbf{k}_2$ modes as shown in Fig. 3b. Two reflected spin waves possess the same y-component of wavevector, satisfying the continuity. The appearance of the two peaks are also confirmed in Fig. 3c, which shows a line plot of the SWaT spectral intensity along the iso-wavenumber line shown by the white dashed line in Fig. 3a ($k_y = 1.18 \times 10^4$ rad cm^{-1}).

In order to rule out bi-reflection of pure elastic waves, we measured magnetic field dependence of the observed bi-reflection. We applied an external field of $H = 0.3$ kOe where the magnetization lies along in-plane orientation. The bi-reflection of spin waves is not observed in the in-plane magnetized film, as shown in the SWaT spectra in Figs. 3d and e. Each SWaT spectrum in Fig. 3d, e show a single peak both before and after the incidence. The incident and reflection angles are found to be the same, meaning the absence of the extraordinary reflection in the in-plane magnetized film. The disappearance of the bi-reflection can also be seen in the line plot of the spectral intensity shown in Fig. 3f. The disappearance of the bi-reflection is attributed to the large frequency difference between the incident and reflected states. In the case of an in-plane magnetized film, the $\mathbf{k}_{in}$ and $\mathbf{k}_2$ modes have the frequency difference greater than 200 MHz because of the anisotropy of the dispersion relation, the energy-momentum relation, of spin waves in the in-plane magnetized film. As a result, conversion between the incident wave and the $\mathbf{k}_2$ mode should be suppressed.

Magneto-elastic hybridization of the observed spin waves. We confirmed that the bi-reflection of spin waves is associated with the coupling between spin and elastic waves by comparing the

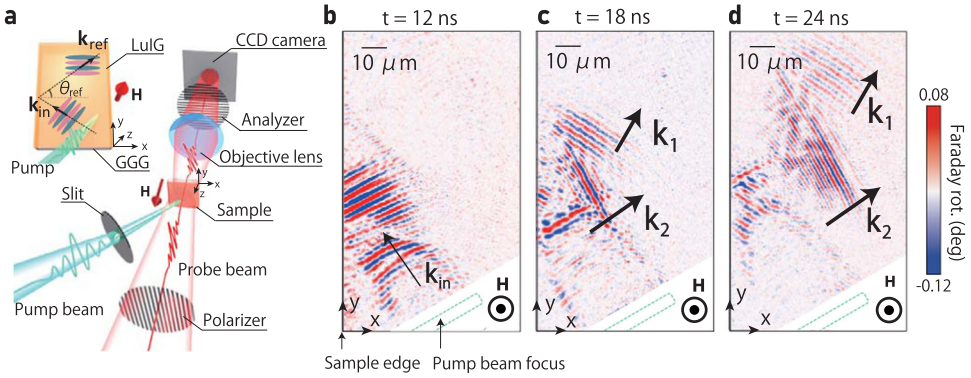

Fig. 2 Experimental setup and time-resolved magneto-optical images of the reflection dynamics. a A schematic of the experimental setup for the time-resolved magneto-optical microscopy. A pulse laser light is divided into pump and probe beams which enter into the sample at different time delay. The pump beam excites spin waves, and the probe beam is detected with a charge-coupled device (CCD) camera. The inset shows a magnified view of the sample configuration. A spin wave is excited by a pump beam focused on the sample. The focus is shaped into an ellipse to determine the propagation direction of the spin wave. The excited spin wave is reflected at the sample edge. **b**–**d** Reflection dynamics of spin waves obtained from the out-of-plane magnetized film at the time delay of 12 ns (**b**), 18 ns (**c**), and 24 ns (**d**). The excited spin wave reflects at the sample edge and splits into two waves with different wavevectors $\mathbf{k}_1$ and $\mathbf{k}_2$.

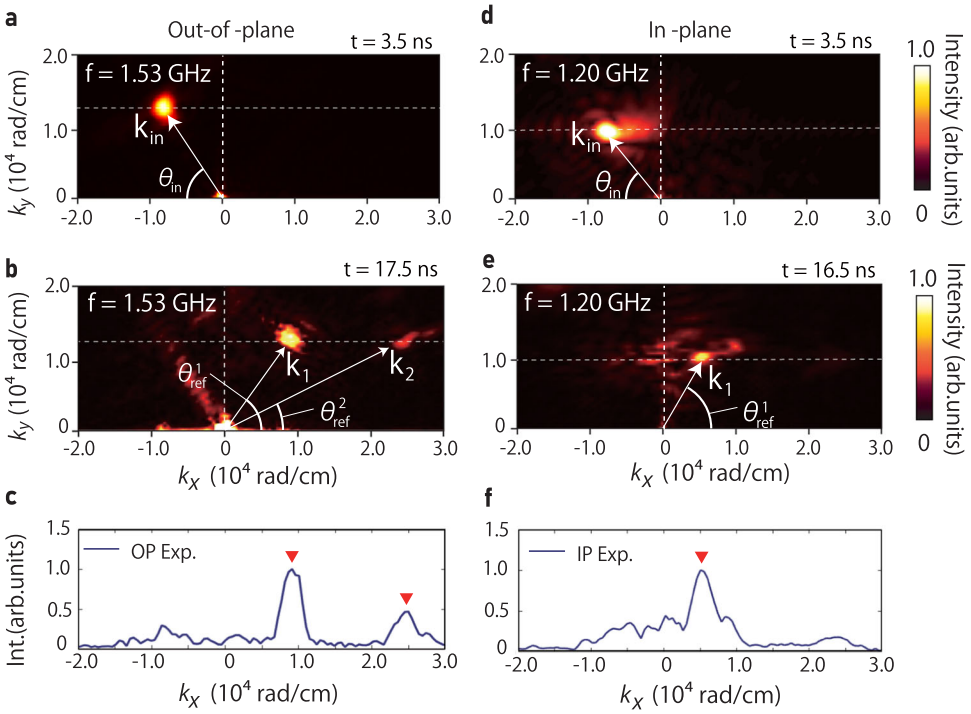

Fig. 3 *k*-space spectra intensity of incident and reflected spin waves. a Cross-sectional view of Spin wave tomography spectra at the frequency $f = 1.53$ GHz obtained by analyzing the series of images taken from the sample with out-of-plane magnetization. **a** (**b**) The spectrum before (after) the incidence of a spin wave. White arrows indicate the wavevector $\mathbf{k} = (k_x, k_y)$ of the incident and reflected waves. Spectrum peak is split into two after the incidence to the sample edge. **c** Spectrum intensity as a function of k_x at $k_y = 1.18 \times 10^4$ (rad cm^{-1}) in the out-of-plane magnetized sample. The spectral intensity has two peaks indicated by red inverted triangles. **d** Cross-sectional view of Spin wave tomography spectra at $f = 1.20$ GHz obtained from the in-plane magnetized sample. **d** (**e**) The spectrum before (after) the incidence of a spin wave. A single spectrum peak appears before and after the incidence. **f** Spectrum intensity as a function of k_x at $k_y = 1.00 \times 10^4$ (rad cm^{-1}) in the in-plane magnetized sample. Contrary to (**c**), only the single peak appears.

SWaT spectra with the calculated dispersion relations. Figure 4a–c show the SWaT spectra for the incident and reflected wave as a function of frequency and wavenumber. The white dashed lines represent dispersion relation of spin waves, longitudinal and transverse modes of elastic waves. Strong peak appears near the crossing between elastic and spin waves, where the magneto-elastic coupling gives birth to the hybridization of the two waves. For the $\mathbf{k}_1$ mode, a strong specrtral peak appears around the crossing between the longitudinal elastic waves and spin waves (Fig. 4b). On the other hand, for the reflected $\mathbf{k}_2$ mode, the intensity is strong around the crossings between the transverse elastic waves and spin waves (Fig. 4c). The result shows that the $\mathbf{k}_2$ mode appears with the aid of the conversion from the longitudinal into the transverse modes of the elastic waves.

To confirm the hybridization of spin waves with elastic waves, we examined the difference between the phase and group velocities of the excited spin waves. For pure elastic sound waves, group and phase velocities should be the same because of the

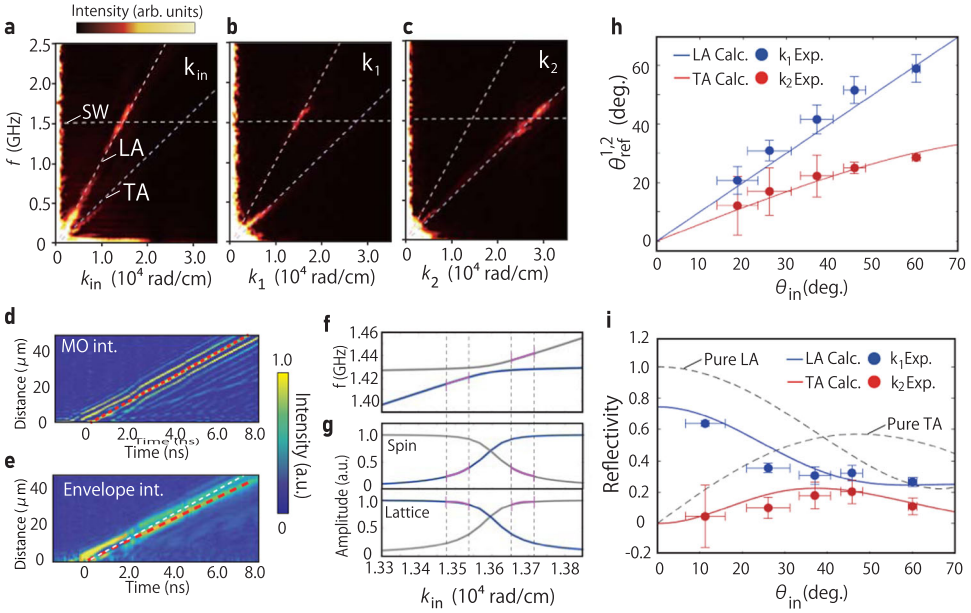

Fig. 4 Spin wave tomography analysis for bi-reflection of spin waves. a Spin wave tomography spectrum for the incident mode as a function of the wavenumber and frequency. White dashed lines indicate the calculated dispersion relation of spin waves (SW), longitudinal (LA), and transverse (TA) elastic waves. The velocity of the longitudinal and transverse elastic waves are 6.5 km s^{-1} and 3.5 km s^{-1}, respectively. **b** Same as (**a**) but along $\mathbf{k}_1$ vector. **c** Same as (**a**) but along $\mathbf{k}_2$. **d** Temporal evolution of a cross-sectional view of the magneto-optical images cut along $\mathbf{k}_{in}$. **e** Same in (**d**) but the envelope data obtained by Hilbert transform are plotted. The slope of the red dashed line in the figure indicates the phase (group) velocity in **d** (**e**). In (**e**), the red dashed line in (**d**) is drawn with a white dashed line for a comparison. **f** Shows the calculated dispersion relation, and (**g**) shows the calculated amplitude of the spin-wave component and the elastic-wave component near the crossing between the longitudinal elastic waves and spin waves. Purple solid curves in (**f**, **g**) between black dashed vertical lines highlight the region having the group velocity obtained from (**e**). **h** Reflection angles plotted as a function of the incident angle. The blue (red) filled circles indicate the reflection angles of the $\mathbf{k}_1$ ($\mathbf{k}_2$) mode. Solid curves show the result of the calculation. The error bars are evaluated from standard deviation of two-dimensional gaussian fitting parameters. **i** Reflectivity of each modes as a function of the incident angle. The blue (red) filled circles indicate the reflectivity of $\mathbf{k}_1$ ($\mathbf{k}_2$) modes. Black dashed curves are the reflectivity of the pure elastic waves. The solid blue (red) curves shows the result of the model calculation. The error bars are evaluated from standard deviation of two-dimensional gaussian fitting parameters.

linear dispersion relation, which is 6.50 km s^{-1} for the longitudinal mode[21]. In the vicinity of the dispersion crossing between elastic and spin waves, on the other hand, the values of group and phase velocity differ to each other because of the anticrossing of the dispersion relation[11,30,31]. Figure 4d shows the temporal evolution of a cross-sectional view for the magneto-optical images along the incident wavevector $\mathbf{k}_{in}$. The signal slope in the intensity map indicates the phase velocity. On the other hand, Fig. 4e shows a cross-sectional view of the magneto-optical signal envelope obtained from real-space Hilbert transform for the magneto-optical images. Here, the signal slope in the intensity map indicates the group velocity (see "Methods"). The phase velocity estimated from the dashed red line in Fig. 4d is 6.51 ± 0.09 km s^{-1}, while the estimated group velocity is 6.05 ± 0.07 km s^{-1}. The result is consistent with the calculated dispersion relation near the crossing between the spin waves and elastic waves (Fig. 4f). Due to the bending of the dispersion relation around the anticrossing, a spin wave has smaller group velocity than phase velocity[30]. Since pure elastic waves have the same phase and group velocities due to its linear dispersion relation, the observed difference in the phase and group velocities demonstrates that the excited spin waves are resonantly coupled with elastic waves. The excited region is indicated in Fig. 4f, g as purple curves. We could not see clear hybridization gap in the spectra between spin waves and elastic waves regardless of the clear coherence of the hybridized spin waves observed in the magneto-optical images. This may be because our frequency resolution is limited to 70 MHz, which is comparable to the expected gap frequency (32 MHz for longitudinal mode and 88 MHz for transverse mode)[31–33].

Discussion

We are now focusing our discussion on the difference between elastic mode conversion and the magneto-elastic mode conversion. Elastic mode conversion should exhibit dependence on the incident angle θ_{in} because θ_{in} changes the ratio of volume and shear strain induced by elastic waves at a sample edge. In the case of oblique incidence of the longitudinal waves, volume strain parallel to the wavevector induces both volume and shear strain at a sample edge[20]. It gives birth to mixing of longitudinal and transverse modes of elastic waves, resulting in elastic mode conversion. In the case of the normal incidence, on the other hand, only volume strain appears at the edge, suppressing elastic mode conversion. Since elastic waves simply pass through in the case of the 90-degree incidence, the conversion efficiency should exhibit a maximum at $0° < \theta_{in} < 90°$. We carried out incident-angle dependence measurement of the bi-reflection of spin waves. Figure 4h shows the relation between the incident angle and reflection angle for the $\mathbf{k}_1$ and $\mathbf{k}_2$ modes in the out-of-plane magnetized sample. According to the continuity of the phase at a boundary, k_y should be kept the same between an incident wave and reflected waves. This boundary condition gives a relation between the incident angle and reflection angle, which is analogous to the case in the light waves and other reflection processes such as Andreev reflection[34]. We measured incident-angle dependence of the reflection angles. The incident angle of the spin wave is controlled by changing the orientation of the elliptic pump-beam focus. The reflection angle is obtained from SWaT spectra in **k**-space by fitting the spectral intensity by using a two-dimensional Gaussian function. Figure 4h shows that the experimentally

obtained relation between the incident and reflection angles is well explained by the calculated relation.

The incident-angle dependence of the reflectivity was found to be different from that of elastic waves. The red (blue) filled circles in Fig. 4i indicate the reflectivity of the $\mathbf{k}_1$ and $\mathbf{k}_2$ modes as a function of the incident angle. The experimentally obtained data do not fit to the calculated rate of the elastic mode conversion, which is plotted as black dashed curves in Fig. 4i.

We constructed a phenomenological model for the efficiency of the conversion. The model is obtained by assuming that hybridized spin waves are reflected by two processes. The first one is the scattering of spin waves at a sample edge. In an out-of-plane magnetized film, the scattering probability is assumed to be constant for any incident angles since the dispersion relation of spin waves is isotropic in the configuration. The second one is the mode conversion of elastic waves. Since the conversion ratio depends on the incident angle, we assumed that the scattering probability depends on the incident angle in the same manner as the elastic mode conversion. Therefore, our scattering Hamiltonian is written as the following equation:

$$\hat{H}_{\mathrm{scat}} = \sum_{\mathbf{k}_{\mathrm{in}},\mathbf{k}_{\mathrm{L}}} A(\theta_{\mathrm{in}})\hat{b}^{\dagger}_{\mathbf{k}_{\mathrm{L}}}\hat{b}_{\mathbf{k}_{\mathrm{in}}} + \sum_{\mathbf{k}_{\mathrm{T}},\mathbf{k}_{\mathrm{in}}} B(\theta_{\mathrm{in}})\hat{b}^{\dagger}_{\mathbf{k}_{\mathrm{T}}}\hat{b}_{\mathbf{k}_{\mathrm{in}}} + \sum_{\mathbf{k}_{\mathrm{L}},\mathbf{k}_{\mathrm{in}}} C\hat{a}^{\dagger}_{\mathbf{k}_{\mathrm{L}}}\hat{a}_{\mathbf{k}_{\mathrm{in}}}, \quad (1)$$

where $\mathbf{k}_{\mathrm{in}}$, $\mathbf{k}_{\mathrm{L}}$, $\mathbf{k}_{\mathrm{T}}$, θ_{in}, $A(\theta_{\mathrm{in}})$, $B(\theta_{\mathrm{in}})$, C, $\hat{a}_{\mathbf{k}}(\hat{a}^{\dagger}_{\mathbf{k}})$, and $\hat{b}_{\mathbf{k}}(\hat{b}^{\dagger}_{\mathbf{k}})$ are the wavevector of an incident wave, the wavevector of reflected longitudinal hybridized spin waves, the wavevector of reflected transverse hybridized spin waves, the incident angle, the reflectivity of pure longitudinal elastic waves, the ratio of conversion from longitudinal elastic waves to transverse elastic waves, the mixing angle of the scattering potential at the edge, the annihilation (creation) operator of spin waves, and the annihilation (creation) operator of elastic waves, respectively. The scattering probability is calculated by using time-dependent perturbation theory.

We calculated the reflectivity by describing the hybridized spin waves as an eigenstate of the total Hamiltonian $\hat{H}_{\mathrm{tot}}$ composed of the spin-wave Hamiltonian $\hat{H}_{\mathrm{s}}$, the elastic-wave Hamiltonian $\hat{H}_{\mathrm{el}}$, and the coupling between spin waves and elastic waves $\hat{H}_{\mathrm{mec}}$ ($\hat{H}_{\mathrm{tot}} = \hat{H}_{\mathrm{s}} + \hat{H}_{\mathrm{el}} + \hat{H}_{\mathrm{mec}}$). The solid red (blue) curve in Fig. 4i represents the calculated reflectivity based on the model. The calculated curves well reproduce the experimentally obtained reflectivity of the $\mathbf{k}_1$ and $\mathbf{k}_2$ modes. The effect of the hybridization between spin waves and elastic waves manifests itself as the decrease in the reflectivity of the $\mathbf{k}_2$ mode. In the vicinity of the crossing points, the amplitude of spin-wave and elastic-wave component exhibits a crossover feature as shown in Fig. 4g[19,30] which decreases the amplitude of the elastic-wave component, leading to suppression of the scattering probability compared to that of the pure elastic-waves' case, consistent with the experimental result. The solid curves in Fig. 4i are calculated by setting the mixing angle $C = 0.8$, which indicates that the scattering probability of spin waves is 20% less than that of elastic waves. The difference in the scattering probability may originate from the reflection loss of spin waves at the sample edge via two magnon scattering, which is allowed when translational symmetry is broken down[6,35].

The material selection for observation of the bi-reflection of spin waves is not limited to $Lu_2Bi_1Fe_{3.4}Ga_{1.6}O_{12}$ because the bi-reflection owes to hybridization between magnon and phonon, which is present in any traditional materials for investigation on spin-wave dynamics, such as yittrium iron garnet and CoFeB.

The bi-reflection accompanies the wavelength conversion for $\mathbf{k}_2$ mode, which extends the controllability of spin waves. In the field of magnonics, where spin-wave propagation and interference play a main role for information transfer and processing, control of wavelength of spin waves is of great importance[36]. Therefore, our result paves a way to control spin waves using mode degree of freedom of elastic waves. Compared with the typical time scale of magnonic devices, several tens of nanoseconds[36–38], the time scale of the wavenumber conversion is comparable, namely 14 ns, which is evaluated from the strength of magneto-elastic coupling of $Lu_2Bi_1Fe_{3.4}Ga_{1.6}O_{12}$ (4.1×10^5 J m^{-3})[33].

Conclusion. In summary, we observed a split of reflected spin waves around an edge of $Lu_2Bi_1Fe_{3.4}Ga_{1.6}O_{12}$: bi-reflection of spin waves, by measuring the reflection dynamics of spin waves by using TRMO microscopy. During reflection around a sample edge, spin waves exhibit clear split into two modes with different wavelengths. We found that the magneto-elastic coupling and a mode degree of freedom inherited from an elastic wave is responsible for the split. The result demonstrates the potential of the mode degree of freedom of elastic waves to control spin-wave propagation in magnetic materials.

Methods

Time-resolved magneto-optical imaging. We used $Lu_2Bi_1Fe_{3.4}Ga_{1.6}O_{12}$ (LuIG) grown on a [001] plane of a gadolinium gallium garnet substrate by liquid phase epitaxy. LuIG is known to exhibit a large magneto-optical effect due to the Bi substitution[26,27]. The sample edge was cleaved mechanically so that it is smooth enough not to diffuse spin waves. Crystallographic orientation does not affect the reflection of the present elastic waves because the sample can be regarded as an isotropic elastic body in the wavelength scale. At the magnetic field of 1350 Oe, the magnetization is nearly saturated. The polar angle of the static magnetization is 0.5 degrees, which was determined by static Faraday rotation measurement. This small tilt of the magnetization allows us to observe spin-wave propagation by magneto-optical Faraday effects in an out-of-plane magnetized film. In the in-plane magnetized sample, due to magnetocrystalline anisotropy, the magnetization form an angle, ϕ, between the sample edge ($//y$) by 17 degrees. We take the z axis as a sample surface normal and x axis as a normal to the sample edge.

The Faraday rotation is measured by the TRMO microscopy which combines pump-and-probe technique and conventional magneto-optical imaging[21,22]. In this method, one can obtain Faraday rotation images with the spatial resolution of 225 nm and temporal resolution of 0.1 ns. We used a 100 fs-duration pulsed light source with the central wavelength of 800 nm and 1 kHz repetition frequency, which was split into pump and probe beams. The central wavelength of the probe beam was tuned to 630 nm with an optical parametric amplifier. The power of probe beam was 50 nJ per pulse. The pump beam was linearly polarized along the y-axis and focused on the sample surface with the length of 25 μm and the width of 3 μm through a metallic slit. The power of pump beam was 1.2 μJ per pulse. The probe beam was linearly-polarized along the y-axis with a Glan-Taylor prism and then was weakly focused on the sample surface. The transmitted probe beam was expanded with an objective lens with the magnification of 20 and then introduced to a magneto-optical imaging system, composed of a half-waveplate mounted on a rotation stage, an imaging lens, an analyzer, and a charge-coupled device (CCD) camera with an another objective lens with the magnification of 2. In this setup, obtained images reflect the rotation angle of the transmitted probe beam. The magnetization dynamics induced by the pump beam was observed by calculating the difference between two images observed with and without the irradiation of the pump beam. The pump beam irradiates the sample and excites spin waves via photo-induced expansion and demagnetization. The excitation of spin waves may be performed via parametric pumping of spin waves with microwave magnetic field, which can excite spin waves hybridized with elastic waves[15].

Time-dependent spectrum analysis, and estimation of group and phase velocities. Time-dependent spectrum analysis was performed via the Fourier transform under the application of the weight function $w = Ae^{-(t-t_c)^2/(2\Delta^2)}$ to the data to extract time-dependent spectra. The full-width-half-maximum of the weight function 2Δ was chosen to 10 ns for all the data analysis. All the analysis were performed by a programs developed with Matlab software by authors.

The estimation of the phase velocity was carried out by fitting the data points as a function of time. Each data point was chosen as the maximum of the cross-sectional data of the Faraday rotation along $\mathbf{k}_{\mathrm{in}}$ in each time frame. The ray intensity of the hybridized spin waves is obtained by using the Hilbert transformation. By calculating the absolute value of the amplitude, one can extract the envelope data. The group velocity was estimated by fitting the data points chosen in the same manner as for obtaining the phase velocity. The calculated dispersion relation and reflectivity plotted in Fig. 4f, the spin-wave and elastic-wave amplitude plotted in Fig. 4g, and reflectivity plotted in Fig. 4i are obtained by using the following parameters, $4\pi M_s = 169.6$ G, $K_{\mathrm{u}} = -7.056 \times 10^3$ erg cm^{-3}, $K_1 =$

6.637×10^2 erg cm^{-3}, where $4\pi M_s$ is a saturation magnetization, K_u is a uniaxial anisotropy constant, K_1 is a cubic anisotropy constant.

Data availability

The data that support the findings of this study are available from the corresponding author upon reasonable request.

Code availability

The code that supports the findings of this study are available from the corresponding author upon request. All the analysis, including spin wave tomography, was performed by codes developed by Matlab 2017b software and Matlab signal processing toolbox.

Received: 27 May 2020; Accepted: 24 September 2020;
Published online: 27 October 2020

References

1. Born, M. & Wolf, E. *Principle Of Optics: Electromagnetic Theory Of Propagation, Interference And Diffraction Of Light* (Cambridge University Press, 1999).
2. Lotem, H. & Laor, U. Low-loss bireflectant (double-reflection) polarization prism. *Appl. Opt.* **25**, 1271–1273 (1986).
3. Burshtein, Z. et al. Refractive-index studies in $Ca_2Ga_2SiO_7$ and $SrLaGa_3O_7$ melilite-type compounds. *J. Opt. Soc. Am. B* **13**, 9 (1996).
4. Kajiwara, Y. et al. Transmission of electrical signals by spin-wave interconversion in a magnetic insulator. *Nature* **464**, 262–266 (2010).
5. Cornelissen, L. J., Liu, J., Duine, R. A., Youssef, J. B. & van Wees, B. J. Long-distance transport of magnon spin information in a magnetic insulator at room temperature. *Nat. Phys.* **11**, 1022–1026 (2015).
6. Gurevich, A. G. & Melkov, G. A. *Magnetization Oscillations And Waves Boca Raton* (CRC Press, Boca Raton,1996).
7. Lindemann, M. et al. Ultrafast spin-lasers. *Nature* **568**, 212–215 (2019).
8. Stigloher, J. et al. Snell's law for spin waves. *Phys. Rev. Lett.* **117**, 037204 (2016).
9. Yu, W., Lan, J., Wu, R. & Xiao, J. Magnetic Snell's law and spin-wave fiber with Dzyaloshinskii-Moriya interaction. *Phys. Rev. B* **94**, 140410(R) (2016).
10. Hioki, T., Tsuboi, R., Johansen, T. H., Hashimoto, Y. & Saitoh, E. Snell's law for spin waves at a 90°, magnetic domain wall. *Appl. Phys. Lett.* **116**, 112402 (2020).
11. Kittel, C. Interaction of spin waves and ultrasonic waves in ferromagnetic crystals. *Phys. Rev.* **110**, 836 (1958).
12. Eshbach, J. R. Spin-wave propagation and the magnetoelastic interaction in Yttrium Iron Garnet. *J. Appl. Phys.* **34**, 1298 (1963).
13. Strauss, W. Elastic and magnetoelastic waves in yttrium iron garnet. *Proc. IEEE* **53**, 1485–1495 (1965).
14. Kikkawa, T. et al. Magnon polarons in the spin Seebeck effect. *Phys. Rev. Lett.* **117**, 207203 (2016).
15. Bozhko, D. A. et al. Bottleneck accumulation of hybrid magnetoelastic bosons. *Phys. Rev. Lett.* **118**, 237201 (2017).
16. Holanda, J., Maior, D. S., Azevedo, A. & Rezende, S. M. Detecting the phonon spin in magnon-phonon conversion experiments. *Nat. Phys.* **14**, 500–506 (2018).
17. Ramos, R. et al. Room temperature and low-field resonant enhancement of spin Seebeck effect in partially compensated magnets. *Nat. Commun.* **10**, 5162 (2019).
18. Yahiro, R. et al. Magnon polarons in the spin Peltier effect. *Phys. Rev. B* **101**, 024407 (2020).
19. Eringen, A. C. & Maugin, G. A. *Electrodynamics Of Continua*. (Springer-Verlag New York Inc., New York, 1990).
20. Leonid, M. & Godin, O. *Acoustics Of Layered Media* (Springer-Verlag Berlin Heidelberg, Heidelberg,1990).
21. Hashimoto, Y. et al. All-optical observation and reconstruction of spin wave dispersion. *Nat. Commun.* **8**, 15859 (2017).
22. Hashimoto, Y. et al. Ultrafast time-resolved magneto-optical imaging of all-optical switching in GdFeCo with femtosecond time-resolution and a μm spatial-resolution. *Rev. Sci. Instr.* **85**, 063702 (2014).
23. Shen, K. & Bauer, G. E. W. Laser-induced spatiotemporal dynamics of magnetic films. *Phys. Rev. Lett.* **115**, 197201 (2015).
24. Hashimoto, Y. et al. Frequency and wavenumber selective excitation of spin waves through coherent energy transfer from elastic waves. *Phys. Rev. B* **97**, 140404(R) (2018).
25. Shelukhin, L. A. et al. Ultrafast laser-induced changes of the magnetic anisotropy in a low-symmetry iron garnet film. *Phys. Rev. B* **97**, 014422 (2018).
26. Helseth, L. E., Hansen, R. W., Il'yashenko, E. I., Baziljevich, M. & Johansen, T. H. Faraday rotation spectra of bismuth-substituted ferrite garnet films with in-plane magnetization. *Phys. Rev. B* **64**, 174406 (2001).
27. Helseth, L. E. et al. Faraday rotation and sensitivity of (100) bismuth-substituted ferrite garnet films. *Phys. Rev. B* **66**, 064405 (2002).
28. Yoshimine, I. et al. Phase-controllable spin wave generation in iron garnet by linearly polarized light pulses. *J. Appl. Phys.* **116**, 043907 (2014).
29. Satoh, T. et al. Directional control of spin-wave emission by spatially shaped light. *Nat. Photon.* **6**, 662–666 (2012).
30. Guerreiro, S. C. & Rezende, S. M. Magnon-phonon interconversion in a dynamically reconfigurable magnetic material. *Phys. Rev. B* **92**, 214437 (2015).
31. Rückriegel, A., Kopietz, P., Bozhko, D. A., Serga, A. A. & Hillebrands, B. Magnetoelastic modes and lifetime of magnons in thin yttrium iron garnet films. *Phys. Rev. B* **89**, 184413 (2014).
32. Flebus, B. et al. Magnon-polaron transport in magnetic insulators. *Phys. Rev. B* **95**, 144420 (2017).
33. Nistor, I., Mayergoyz, I. D. & Rojas, R. Optical study of magnetostriction in (Bi, Ga)-substituted garnet thin films. *J. Appl. Phys.* **98**, 073901 (2005).
34. Žutić, I. & Sarma, S. D. Spin-polarized transport and Andreev reflection in semiconductor/superconductor hybrid structures. *Phys. Rev. B* **60**, R16322(R) (1999).
35. Nemarich, J. Contribution of the two-magnon process to magnetostatic-mode relaxation. *Phys. Rev.* **136**, A1657 (1964).
36. Chumak, A. V., Vasyuchka, V. I., Serga, A. A. & Hillebrands, B. *Nat. Phys.* **11**, 453–461 (2015).
37. Serga, A. A., Demokritov, S. O. & Hillebrands, B. Self-generation of two-dimensional spin-wave bullets. *Phys. Rev. Lett.* **92**, 117203 (2004).
38. Brächer, T. et al. Time- and power-dependent operation of a parametric spin-wave amplifier. *Appl. Phys. Lett.* **105**, 232409 (2014).

Acknowledgements

The authors thank B. Hillebrands and A.A. Serga and Y. Oikawa and R. Tsuboi for valuable discussions. This work was financially supported by JST-ERATO (No. JPMJER1402) from JST, Japan, the Grant-in-Aid for Scientific Research (S) (No. JP19H05600) from JSPS KAKENHI, Japan, and World Premier International Research Center Initiative (WPI), Japan. T.H. is supported by JSPS through a research fellowship for young scientists (No. 18J21004) and acknowledges the support from GP-Spin at Tohoku University.

Author contributions

T.H. performed the measurement, analyzed the data, and developed the theoretical model with input from Y.H. and E.S. T.H. and E.S. planned and E.S. supervised the study. T.H. wrote the paper with review and input from Y.H. and E.S. All the authors discussed the results and explanation of the experiments.

Competing interests

The authors declare no competing interests.

Additional information

Supplementary information is available for this paper at https://doi.org/10.1038/s42005-020-00455-6.

Correspondence and requests for materials should be addressed to T.H.

Reprints and permission information is available at http://www.nature.com/reprints

Publisher's note Springer Nature remains neutral with regard to jurisdictional claims in published maps and institutional affiliations.